Journal of Power Sources 196 (2011) 4741–4746

Contents lists available at ScienceDirect

Journal of Power Sources

journal homepage: www.elsevier.com/locate/jpowsour

New three-dimensional electrode structure for the lithium battery: Nano-sized γ-Fe_2O_3 in a mesoporous carbon matrix

Miki Nagao, Michiko Otani, Hiroki Tomita, Sho Kanzaki, Atsuo Yamada, Ryoji Kanno*

Department of Electronic Chemistry, Interdisciplinary Graduate School of Science and Engineering, Tokyo Institute of Technology, 4259 Nagatsuta, Midori, Yokohama 226-8502, Japan

ARTICLE INFO

Article history:
Received 14 July 2010
Received in revised form
26 December 2010
Accepted 19 January 2011
Available online 26 January 2011

Keywords:
Lithium secondary batteries
Mesoporous carbon
Iron oxide

ABSTRACT

A new electrode structure based on a three-dimensional mesoporous matrix was developed. Nanoparticles of γ-iron oxide (Fe_2O_3) were introduced into the mesopores of a carbon matrix (mesoporous carbon, CMK-3) by oxidizing metallic iron, which was electroplated in the matrix. The resulting structure was found to have a high charge–discharge capacity when used as the positive electrode of a lithium battery. The iron oxide nanoparticles bonded tightly to the electrically conductive electrode framework, and showed a high activity for the electrochemical reaction: $Fe_2O_3 + 6Li \rightarrow 3Li_2O + 2Fe$.

1. Introduction

Since the lithium-ion configuration, consisting of carbon anodes and intercalated cathodes, has been widely accepted for lithium secondary batteries, significant efforts have been devoted to attaining high energy and power densities for improved energy storage systems [1–4]. In particular, recent progress in pure electric vehicles (EV) requires battery systems capable of both high power operation and a high capacity. The power characteristics of battery systems are closely related to the nature of their electrode reactions, so a rapid charge transfer process at the electrode surface is necessary. Electrodes with a high surface area and a highly conductive matrix may improve the electrochemical reactions, and may be suitable for high power density battery systems. There are several possible methods of improving the capacity of electrodes, such as the use of new materials in the intercalation reactions and developing nanoparticles of conventional electrode materials. We recently focused on iron oxide cathode materials, because iron-based materials are ideal cathodes for lithium secondary batteries due to their low cost and low environmental impact, compared with cobalt- or nickel-based cathode materials containing heavy metal active reaction centers [5,6]. Nano-sized γ-Fe_2O_3 showed a high reversible capacity of 200 mAh g^{-1}, with a reaction mechanism characteristic of a nano-sized material. The nano-sized particles make the following reactions possible: (i) reversible lithium intercalation into the host structure [6], (ii) reversible phase transformation between the host and the intercalated phase [7], and (iii) reversible reaction between the iron metal and iron oxides [8–10], which is similar to a reaction previously reported for iron oxide [11]. These mechanisms were not observed in the bulk materials. Therefore, the nano-sized iron oxides are attractive candidates for future electrode materials [12,13].

However, nano-sized materials have practical difficulties in their handling and in measuring electronic conduction of their small particles. In order to obtain high energy and power densities, it is necessary to improve the utilization ratio of the electrodes, while reducing the resistance at the electrolyte/electrode interface. The best solution is to use electrodes with both high electrical conductivity and high surface area at the electrode–electrolyte contact. The mesoporous electrode is a promising candidate for this purpose. Particularly, mesoporous carbon (CMK-3) has a high surface area with a homogeneous distribution of meso-sized pores [14] and a high electronic conductivity [15]. High lithium storage capacity was proposed for a lithium anode material using the CMK-3, because the carbon system usually provides cell voltages near 0 V vs. Li [16]. On the other hand, no extensive research has been done on applying these materials to positive oxide electrodes, while the carbon matrix is reported to be suitable for sulfur cathode material [17]. We attempted to use a three-dimensional matrix for a nanoparticle cathode.

In the present study, a new electrode structure of mesoporous carbon and iron oxide was examined as a positive electrode material with a high lithium storage capacity and a high rate capability the battery reaction. The "meso-nano" composite electrode was synthesized by electroplating in an aqueous solution, which

* Corresponding author.
E-mail address: kanno@echem.titech.ac.jp (R. Kanno).

0378-7753/$ – see front matter © 2011 Elsevier B.V. All rights reserved.
doi:10.1016/j.jpowsour.2011.01.066

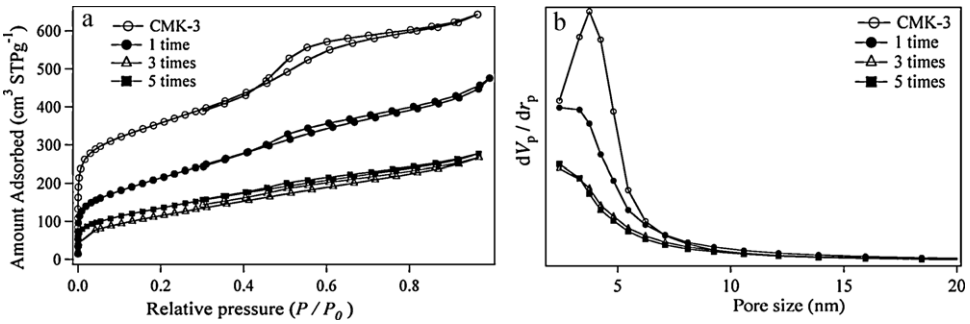

Fig. 1. N_2 adsorption isotherms (a) and pore distribution (b) of mesoporous carbon (CMK-3) and samples prepared by electrolysis: CMK-3, 1 electrolytic deposition, 3 depositions, and 5 depositions.

resulted in iron nanoparticles embedded in the mesopores of the carbon matrix. The synthesis, characterization, charge–discharge behavior, and reaction mechanisms of this electrode are discussed below.

2. Experimental

CMK-3 was synthesized using SBA-15 silica as a template and sucrose as a carbon source [18]. An SBA-15 sample was prepared using a triblock copolymer (P-123), $EO_{20}PO_{70}EO_{20}$ (Aldrich) as a surfactant, and tetramethyl orthosilicate (TMOS, Kanto chem. 95%) as a silica source.

Iron metal was deposited on the mesoporous carbon by electrolysis, using a previously reported method [19]. A mixture of CMK-3 and PTFE with a weight ratio of 95:5 was pressed into a pellet and placed on the carbon tape as a cathode for electrolysis. An anode was an Al plate with a surface area of 5 cm^2. The electrolyte solution was prepared as follows: 36.6 g of iron sulfate hydrate ($FeSO_4{\cdot}7H_2O$) and 12.5 g of iron chloride hydrate ($FeCl_2{\cdot}4H_2O$) were dissolved in 28.9 ml of H_2O. The mixture was stirred at 313 K, and electrolysis was carried out with a current of 2.85 mA for 1710 s. After the electrolysis, the pellet was crushed, washed with distilled water, and dried. This process was repeated several times and then the sample was oxidized at 250 °C for 1 h under oxygen gas flow.

The samples were characterized by scanning electron microscopy (SEM) (Hitachi Co., S-4700, S-4800), X-ray diffraction (XRD) (Rigaku, RU-200, 12 kV, Cu Kα radiation; BRUKER AXS K. K., D8 FOCUS, 35 kV, Co Kα radiation), small-angle X-ray scattering (SAXS) (Rigaku, Ultima-IV, 40 kV, Cu Kα radiation), ICP (LEEMAN LABS/JEOL DATUM, Prodigy and SHIMAZU, ICPS-8100), and TG–DTA (SII, TG/DTA6300, EXSTAR6000) with a heating rate of 5 °C min^{-1} up to 500 °C in air. The nitrogen adsorption and desorption isotherms (BET, BEL JAPAN, INC., BELSORP-mini-II) were measured after the sample was pretreated at 150 °C for 1 h in vacuum. The BET data were analyzed by the BJH (Barrett–Joyner–Halenda) method using the Halsey equation for multilayer thickness. The pore size distribution curves were obtained from analysis of the adsorption branch of the isotherm. The pore volume was taken at the $P/P_0 = 0.952$ single point. The electrochemical characteristics were measured at 25 °C with a 2032 coin-type cell or a test cell (Hohsen Co.) with a lithium metal anode. The cathode in these cells consisted of a mixture of 50 mg of sample, 10 mg of acetylene black (Denki Kagaku Kogyo K. K.), and 0.1 mg of Teflon powder, pressed into a tablet 11 mm in diameter under a pressure of 12 MPa. The electrode was dried at 150 °C in a vacuum before the electrochemical tests. The pellet of the cathode was put on an Al plate to take an electrical contact. A spacer and a spring were used in the anode side. The electrolyte was ethylene carbonate (EC)–diethyl carbonate (DEC) with a molar ratio of 3:7 as a solvent and a supporting electrolyte of 1 M $LiPF_6$. The charge-and-discharge experiments were performed at 25 °C. Cyclic voltammogram (CV) of all samples (CMK-3, γ-Fe_2O_3/CMK-3 and pure γ-Fe_2O_3) was examined using a lithium metal as the reference and counter electrodes with a scan rate of 0.1 mV s^{-1} and a scan range between 1 and 4 V.

3. Results and discussion

Fig. 1 shows the N_2 adsorption isotherms and pore distributions of mesoporous carbon (CMK-3) samples prepared by one, three, and five repeated cycles of electrolysis. The isotherm of the CMK-3 composites is considered as a combination of the I and IV IUPAC types isotherm. The patterns of the isotherm I and IV correspond to the existence of micro-size pore and meso-size pore, respectively. During the electrolysis process, the type I and type IV behavior decreased with the repetitions of the process. This indicated that the micro-pore decreased and the meso-pores almost disappeared. Moreover, the surface area decreased with the electrolysis process, indicating that the iron filled the pores, and began to cover the surface of the particles. The isotherm of the sample after the five times deposition was similar to those of the three times deposition, indicating that the iron did not placed into the meso-pore after the three times electrolysis process. The pore distribution function shown in Fig. 1(b) indicated that pores with a diameter of 3–4 nm in the mesoporous carbon disappeared for all electrolysis samples. Fig. 2 shows small-angle X-ray scattering (SAXS) profiles of CMK-3 with iron deposited in the structure. The peak at $Q = 0.069$ $Å^{-1}$ corresponds to the distance between the axial centers of the carbon rods. The distance of ~90 Å is calculated according to the equation, $d = 2\pi/Q$. The intensity of the peak decreased with increasing electroplating of iron. This indicates that the iron coating on the surface of the rod obscured the boundaries of the rods. The SAXS profile of CMK-3 between $Q = 0.15$ and 0.5 $Å^{-1}$ had an additional scattering, which contained information on the form and the surface of the carbon rods and also information on the pore. The scattering decreased and the slope values converged with increasing repetitions of iron coating. The pore size decreased and the surface became uniform due to iron particles adhered to the surface. Fig. 3 shows wide-angle X-ray diffraction patterns for CMK-3 after iron deposition. The X-ray diffraction patterns of samples after the electroplating contained a peak due to γ-Fe_2O_3 at $2\theta = 41°$. The peak was recognized clearly after three times electroplating and exposing to air. This indicates that iron immediately changed to the iron oxide after the electroplating. Therefore, the sample after three times coating was oxidized and transformed completely from Fe to γ-Fe_2O_3. The lattice parameters of the carbon changed from $a = 2.070$ Å and $c = 7.912$ Å for the original carbon to $a = 2.082$ Å and $c = 7.956$ Å after three-times repetitions of the iron coating process. The change in the interlayer distance of the graphene layers indicates an interaction between the carbon layer and the iron oxides. The sample

Table 1
BET surface area, pore volume, distance between the axial centers of the rods (d_{rods}), pore size, and wall thickness of mesoporous carbon and iron oxide composite.

Sample	BET surface area, s ($m^2\ g^{-1}$)	Pore volume, v ($m^3\ g^{-1}$)	d_{rods}, l (nm)	Pore size, l (nm)
CMK-3	1077	0.99	9.1	3.7
Composite (1 time)	727	0.73	9.1	3.0
Composite (3 times)	406	0.41	9.1	2.4
Composite (5 times)	452	0.43	–	2.0

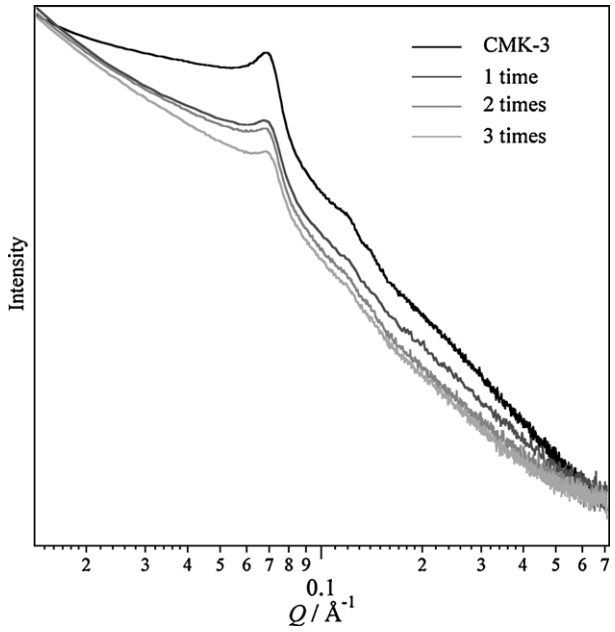

Fig. 2. Small-angle X-ray scattering patterns of mesoporous carbon (CMK-3) and samples prepared by electrolysis.

after 3 times coating was oxidized at 250 °C 1 h in O_2 to complete the reaction form Fe to Fe_2O_3. The distance between layers and the structure of graphene were d_{002} = 3.94 Å and d_{10} = 2.07 Å, respectively. The distance decreased than CMK-3 at 3rd times by the electroplating. The structure of graphene slightly changed. The structure of carbon is not affected by the heating temperature after electroplating. The structure change is attributed to an interaction between carbon and iron oxide. Table 1 summarizes the BET surface area, pore volume, distance between the axial centers of the rods (d_{rods}) and pore size of the mesoporous carbon and of samples after electrolysis. The BET surface decreased with the electroplating process to three times, and then increased at the five times plating. The decrease in the surface area corresponds to the complex surface of carbon being felled with the iron oxide and the decrease in the pore volume. The increase in the surface area at the five times coating indicates that the surface became more complex due to the iron oxide particles deposited on the surface of the samples. This caused the decrease in the pore volume and the increase in the complexity of sample surface, which correspond to the changes in the adsorption isotherms. The Mössbauer spectra in Fig. 4 from samples after electrolysis showed a doublet of a single iron component with an isomer shift of IS = 0.27 mm s^{-1} and a quadrupole splitting of QS = 0.95 mm s^{-1}, which is consistent with the Fe^{3+} state. Therefore, the iron deposited in and on the CMK-3 was oxidized in O_2 to Fe^{3+}. Trivalent iron oxide normally shows quadrupole splitting; the doublet of spectra indicated a disappearance of the internal magnetic field, suggesting super-paramagnetism due to nanoparticle effects. The iron content in the final product was determined by chemical analysis using ICP. For example, the sample after three repetitions of the electroplating process had an iron content of about 30% of the total sample weight. Therefore, composite materials of mesoporous carbon and nano-sized iron oxide were successfully synthesized in the present study. Fig. 5 shows the structure of a mesoporous carbon/iron oxide composite electrode. Iron oxide was deposited in the mesopores of the carbon matrix while the composite structure had pores around 2 nm in size. After the electroplating, all of the deposited iron was converted to amorphous iron oxide by O_2. Fig. 6 shows SEM photographs of mesoporous carbon and composite electrodes heated at 250 °C in O_2. The surface of the carbon matrix was covered by small particles with a diameter of 2–3 nm and a length of 10 nm. No segregation of these nanoparticles was observed after heat treatment. EDX analysis indicated a homogeneous distribution of iron on the surface.

Fig. 7 shows cyclic voltammograms (CVs) of CMK-3, nano-sized γ-Fe_2O_3 particles [6], and a composite electrode. The composite electrode had a broad oxidation peak around 2.3 V and a reduction peak around 1.5 V, which were consistent with the redox couple of Fe(III)/Fe(II). The CV data of the composites contain the electrochemical reaction of both the nano-size iron oxide and carbon. There was an interaction between the iron oxide and the carbon layer, which is indicated by the XRD data shown in Fig. 3; the dis-

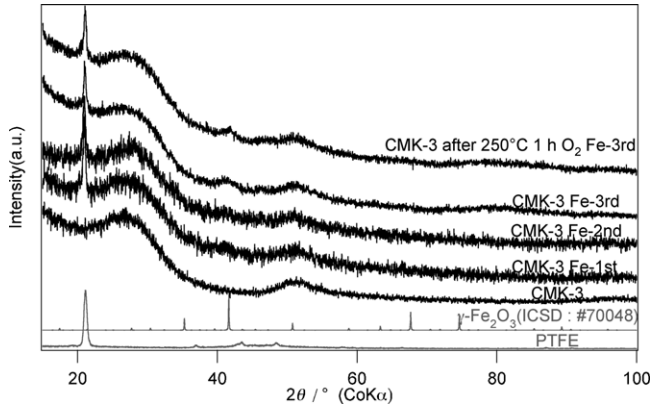

Fig. 3. X-ray diffraction patterns of CMK-3, samples prepared by repeating electrolysis three times, and a sample prepared by heat treatment at 250 °C.

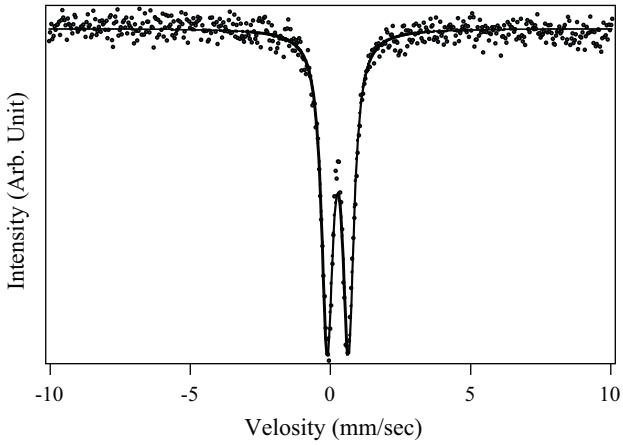

Fig. 4. Mössbauer spectra of the composite electrode after electrolysis.

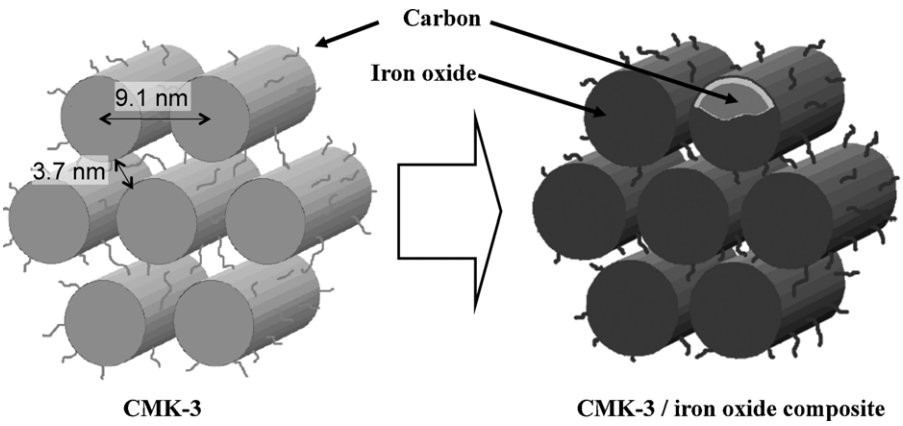

Fig. 5. Schematic drawing of a composite electrode of iron oxide on a mesoporous carbon support.

tance between the layers of CMK-3 changed by the electroplating, and the charge–discharge mechanism of the composites might be different from that of the pristine iron oxide. The change in the mechanism is also indicated by a slightly lower cell voltage for the composite electrodes than those of the original iron oxide. On the other hand, the pristine carbon CMK-3 matrix also showed the charge–discharge property at lower voltage region in Fig. 8(a). However, its capacity of the second cycle was only 250 mAh g^{-1} with a cut-off voltage of 0.3 V; the reversible capacity is mostly due to the capacity of below 1.0 V and the capacity value is much lower than that of the composite electrodes. This indicates that the large reversible capacity of the composite electrodes is mainly due to the iron oxides. Its mechanism is influenced by the mixing process with the carbon matrix and might be different from that of the pristine mero-porous carbon, CMK3.

Fig. 8(b) shows charge–discharge curves of the composite electrode with a current density of 0.1 mA cm^{-2} and cut-off voltages of 1.0 and 4.0 V. The composite electrode had a much higher capacity than that of the γ-Fe_2O_3 nanoparticles (230 mAh g^{-1}) [6]. The capacity was calculated for both the mesoporous carbon/iron oxide composite sample and iron oxide (Fe_2O_3). As the CV experiments indicated that only the iron oxide participated in the electrochemical reactions, a capacity value based on Fe_2O_3 was used. It is surprising that the first discharge capacity exceeded 1100 mAh g^{-1}, which is much higher than the theoretical values of 340 and 170 mAh g^{-1} for electrode reactions (1) and (2), respectively.

$$Fe_2O_3 + 2Li \rightarrow Li_2Fe_2O_3 \quad (1)$$

$$Fe_2O_3 + Li \rightarrow LiFe_2O_3 \quad (2)$$

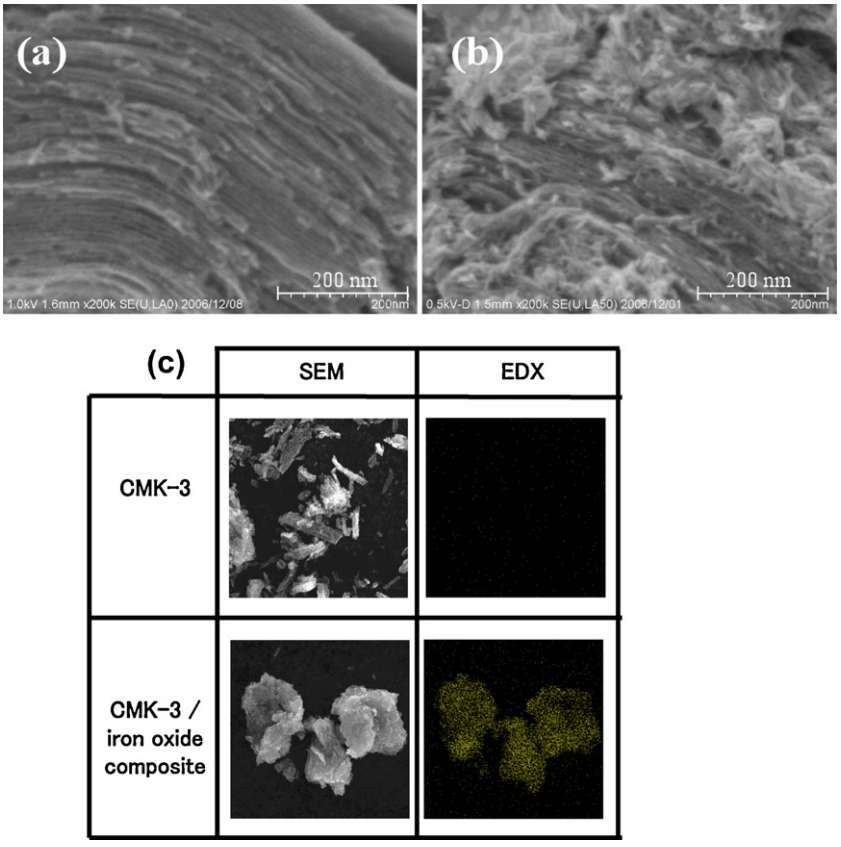

Fig. 6. SEM (a and b) and EDX (c) images of mesoporous carbon (CMK-3) (a) and CMK-3/iron oxide composite (b). The iron distribution was mapped for the EDX image (c).

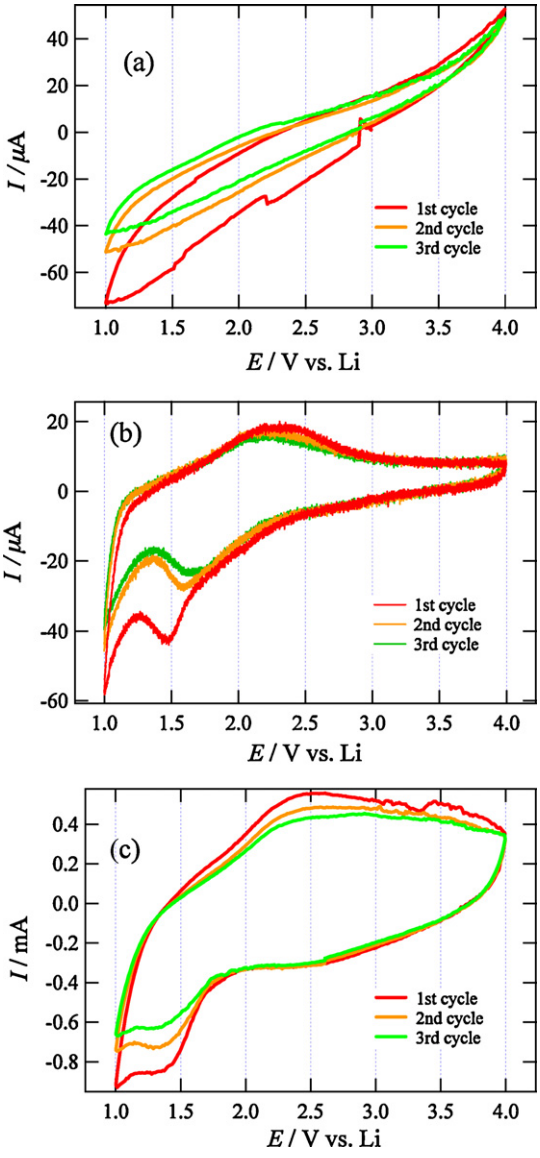

Fig. 7. Cyclic voltammograms of (a) CMK-3, (b) γ-Fe_2O_3 (nanoparticle), and (c) γ-Fe_2O_3/CMK-3. Scan rate: 0.1 mV s^{-1}.

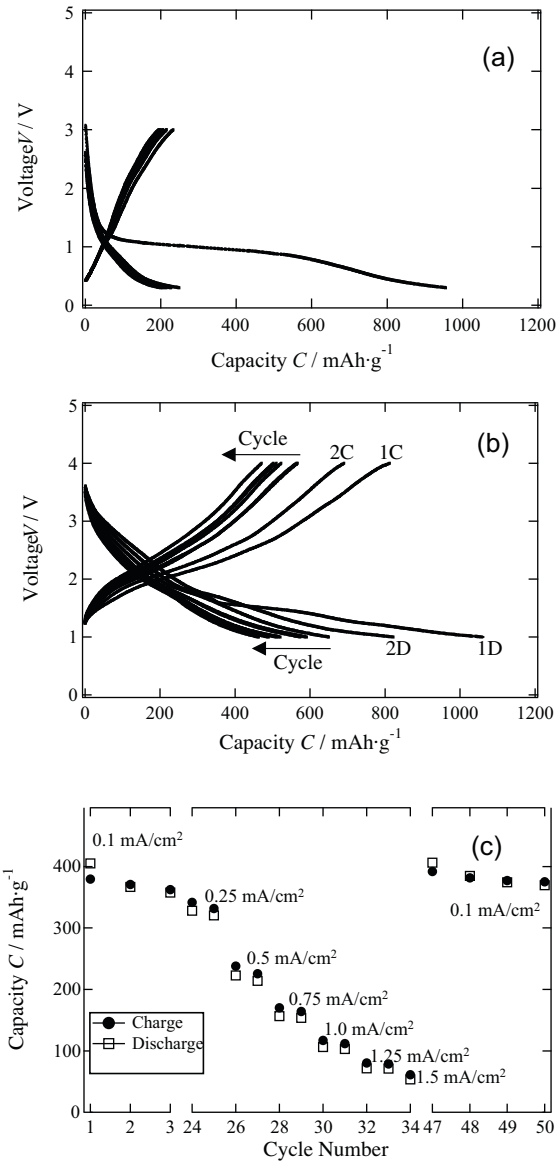

Fig. 8. (a) Charge–discharge curves for CMK-3. Current density: 0.1 mA cm^{-2} between 0.3 V and 3.0 V. (b) Charge–discharge curves for mesoporous carbon/iron oxide composite. Current density: 0.1 mA cm^{-2} between 1.0 V and 4.0 V. Active material: Fe_2O_3. (c) Cycling performance of mesoporous carbon/iron oxide composite between 1.0 V and 4.0 V. The anode was LiCMK-3 (Li_xC_6: $x = 5.4$). The capacity changes with current density are indicated during the cycling experiments.

The capacity obtained is comparable to the theoretical value of 1020 mAh g^{-1} for the following reaction.

$$Fe_2O_3 + 6Li \rightarrow 3Li_2O + 2Fe \quad (3)$$

Recently, Ito and co-workers reported a large-capacity iron oxide for high temperature operation, which exceeded 1000 mAh g^{-1} [20]. They proposed a reaction mechanism in which the iron was reduced to a metallic state. However, the cell voltages of our system exceeded 1.0 V, which could not be provided by a redox couple of Fe(0)/Fe(II). The Mössbauer spectra of the discharged sample indicated a mixed-valence state of Fe(II)/Fe(III). The refined parameters are summarized in Table 2. Assuming that the redox couple of Fe(II)/Fe(III) participates in all of the charge–discharge reactions, the capacity calculated from the Mössbauer data was 84 mAh g^{-1}, which is much smaller than the capacities observed in our experiments. Similar discrepancies between the charge–discharge capacity and valence state obtained by Mössbauer spectroscopy were previously reported for $LiFeO_2$ with an β-$NaMnO_2$ type and a holandite structure [21,22], and layered lithium manganese iron oxide [23,24]. Further studies on the charge–discharge mechanism are necessary to understand the huge capacity obtained for this iron oxide system. The charge–discharge characteristics were measured as a function of current in the range of 0.1–1.5 mA cm^{-2}, corresponding to a C-rate of 0.14–2.1. Li/CMK-3 ($Li_{5.6}C_6$) was used for the anode material to decrease the irreversible capacity. Although the capacity decreased with increasing charge/discharge rates, a reversible capacity of ~100 mAh g^{-1} was observed for a current rate of 1.5 mA cm^{-2}.

Table 2
Fitting parameters of Mössbauer spectra of mesoporous carbon/iron oxide composite, before and after the electrochemical discharge experiments.

	Species	Quotient	IS	QS
Before discharge	Fe(III)		0.271	0.955
After discharge	Fe(II)	25.7	0.741	1.770
	Fe(II)	74.3	0.326	0.671

Discharge voltage is 1.0 V vs. Li.

The decrease of the charge–discharge capacities in Fig. 8(a) indicated that the contact between Fe_2O_3 and carbon was difficult to change the volume of Fe_2O_3 through the reaction, Fe(III)/Fe(II) and the carbon contributed to the electrochemical property and trapped lithium around 1 V. Therefore, in Fig. 8(c), the cycling performances were better due to the reaction to which the carbon did not contribute. The discharge capacities of the cell were 405 and 220 mAh g^{-1} at 0.1 and 0.5 C, respectively. The cell with γ-Fe_2O_3 nanoparticle showed 200 and 170 mAh g^{-1} for 0.1 and 0.5 C, respectively. The rate performance of γ-Fe_2O_3/CMK-3 was then improved using the composite of γ-Fe_2O_3 nanoparticle and CMK-3.

There are several important factors associated with lithium battery reactions; (i) the bulk intercalation reaction, (ii) the reversible oxidation–reduction reaction between a metal oxide and a metal (i.e. 0 valence state), (iii) adsorption at the surface. Nanoscale size effects in the electrode reaction were clarified for γ-Fe_2O_3 as follows: (i) reversible lithium (de-)intercalation into the spinel structure with iron in the tetrahedral sites [6], and (ii) a reversible phase transition between the spinel and the disordered rock-salt structures [7]. A reversible process with an electrode reaction, shown in Eq. (3) was previously reported for simple oxide nanoparticles, such as CoO and FeO [11], in which reduction to the metal resulted in a high capacity and a low charge–discharge potential below 1.0 V vs. Li. α-Fe_2O_3 also showed a high capacity with this reaction mechanism down to cell voltages of 0 V [8–10]. On the other hand, the importance of the surface adsorption of lithium was discussed for Fe_2O_3–SnO_2 composite cathode materials [5]. Our mesoporous carbon/iron oxide composite electrode had an extremely high charge–discharge capacity above cell voltages of 1.0 V, with no indication of the reduction to iron metal in the Mössbauer data. The role of the nanoparticle surface is important in the charge–discharge reactions.

In conclusion, we synthesized a composite electrode of mesoporous carbon (CMK-3) and iron oxide nanoparticles using electrolysis. The mesopores of the carbon structure were almost completely filled with iron oxide nanoparticles, which formed a close contact between the highly electrically conductive carbon matrix and the cathode materials. The composite structure enabled a high utilization ratio of the iron oxide electrode and high charge–discharge reaction rates. This new three-dimensional composite electrode structure should provide a higher utilization of nanomaterial electrodes. Furthermore, a wide range of composite structures is possible through changing the configuration of the mesoporous carbon, which may improve the energy and current densities of the electrodes by reducing the volume content of their carbon matrix.

References

[1] K. Mizushima, P.C. Jones, P.J. Wiseman, J.B. Goodenough, Mater. Res. Bull. 15 (1980) 783–789.
[2] H. Ikeda, S. Narukawa, H. Nakajima, Japan Pat., 62-23433, B (1987).
[3] R. Kanno, Y. Takeda, T. Ichikawa, K. Nakanishi, O. Yamamoto, J. Power Sources 26 (1989) 535–543.
[4] M. Mohri, N. Yanagisawa, Y. Tajima, H. Tanaka, T. Mitate, S. Nakajima, M. Yoshida, Y. Yoshimoto, T. Suzuki, H. Wada, J. Power Sources 26 (1989) 545–551.
[5] T. Matsumura, N. Sonoyama, R. Kanno, M. Takano, Solid State Ionics 158 (2003) 253–260.
[6] S. Kanzaki, T. Inada, T. Matsumura, N. Sonoyama, A. Yamada, M. Takano, R. Kanno, J. Power Sources 146 (2005) 323–326.
[7] S. Kanzaki, A. Yamada, R. Kanno, J. Power Sources 165 (2007) 403–407.
[8] B.T. Hang, I. Watanabe, T. Doi, S. Okada, J.-I. Yamaki, J. Power Sources 161 (2006) 1281–1287.
[9] D. Larcher, C. Masquelier, D. Bonnin, Y. Chabre, V. Masson, J.-B. Leriche, J.-M. Tarascon, J. Electrochem. Soc. 150 (2003) A133–A139.
[10] D. Larcher, D. Bonnin, R. Cortes, I. Rivals, L. Personnaz, J.-M. Tarascon, J. Electrochem. Soc. 150 (2003) A1643–A1650.
[11] P. Poizot, S. Laruelle, S. Grugeon, L. Dupont, J.-M. Tarascon, Nature 407 (2000) 496–499.
[12] S. Komaba, K. Suzuki, N. Kumagai, Electrochemistry 70 (2002) 506–510.
[13] M. Hibino, J. Terashima, T. Yao, J. Electrochem. Soc. 154 (2007) A1107–A1111.
[14] D.Y. Zhao, Science 279 (1998) 548–552.
[15] L. Wang, S. Lin, K. Lin, C. Yin, D. Liang, Y. Di, P. Fan, D. Jiang, F.-S. Xiao, Micropor. Mesopor. Mater. 85 (2005) 136–142.
[16] H. Zhou, S. Zhu, M. Hibino, I. Honma, M. Ichihara, Adv. Mater. 15 (2003) 2107–2111.
[17] X. Ji, K.T. Lee, L.F. Nazar, Nat. Mater. 8 (2009) 500–506.
[18] S. Jun, S.H. Joo, R. Ryoo, M. Kruk, M. Jaroniec, Z. Liu, T. Ohsuna, O. Terasaki, J. Am. Chem. Soc. 122 (2000) 10712–10713.
[19] Y. Nobumoto, K. Kumota, S. Yoshuhara, T. Shirakashi, W. Oikawa, N. Kudoh, 109th The Surface Finishing Society Symposium, 2004, p. 17A26.
[20] T. Kato, K. Nakazawa, K. Fujimoto, S. Ito, The 47th Battery Symposium in Japan, 2006, p. 3F20.
[21] T. Matsumura, R. Kanno, Y. Inaba, Y. Kawamoto, M. Takano, J. Electrochem. Soc. 149 (2002) A1509–A1513.
[22] T. Shirane, R. Kanno, Y. Kawamoto, Y. Takeda, M. Takano, T. Kamiyama, F. Izumi, Solid State Ionics 79 (1995) 227–233.
[23] M. Tabuchi, A. Nakashima, K. Ado, H. Sakaebe, H. Kobayashi, H. Kageyama, K. Tatsumi, Y. Kobayashi, S. Seki, A. Yamanaka, J. Power Sources 146 (2005) 287–293.
[24] M. Tabuchi, A. Nakashima, K. Ado, H. Kageyama, K. Tatsumi, Chem. Mater. 17 (2005) 4668–4677.